

Influence of carrier injection on the metal-insulator transition in electron- and hole-doped $R_{1-x}A_x\text{NiO}_3$ perovskites

J. L. García-Muñoz and M. Suaaidi

Instituto de Ciencia de Materiales de Barcelona, Consejo Superior de Investigaciones Científicas, E-08193 Bellaterra, Spain

M. J. Martínez-Lope and J. A. Alonso

Instituto de Ciencia de Materiales de Madrid, Consejo Superior de Investigaciones Científicas, Serrano 113, E-28003 Madrid, Spain

(Received 27 June 1995)

The influence of the distortion and the extra-carrier injection upon the first-order metal-insulator transition has been investigated in electron- and hole-doped series of $R_{1-x}A_x\text{NiO}_3$ perovskites. The temperature-driven metal-insulator transition is progressively suppressed by either electron or hole doping of these charge-transfer nickelates. The suppression rates dT_{MI}/dx experimentally found are strongly independent on the cationic dopant (A : Sr^{2+} , Ca^{2+} , Th^{4+} , Ce^{4+}) and not only on its ionic valence. The origin of such differences is proven to be twofold: first, the mean size of atoms at the rare-earth (R) site, that modifies the Ni-O-Ni bond angle, and second, intrinsic electronic effects associated with the carrier injection (electron or holes) into the Ni-O bond. Analysis of the structural modifications and resistivity data have allowed us to separate both effects. By applying the appropriate R -size corrections, the obtained bare suppression rates for the intrinsic effects of doping are $\partial T_{\text{MI}}/\partial x \approx -3200$ K for divalent cations (hole doping) and $\partial T_{\text{MI}}/\partial x \approx -1200$ K in the case of tetravalent substitutions (electron doping). It is shown that the injection of holes probably in oxygen p -like impurity states is about three times more effective than supplying electrons into $3d$ -like impurity bands for the closing of the charge-transfer gap. The origin of the reported electron-hole asymmetry is also discussed.

I. INTRODUCTION

The electronic structure of transition-metal (TM) oxides has been a controversial topic during the past 50 years. To this extensive group of materials belong systems such as VO_2 , $\text{V}_N\text{O}_{2N-1}$, Ti_2O_3 , the superconducting cuprates, and the ferromagnetic perovskites with colossal magnetoresistance $R_{1-x}A_x\text{MnO}_3$. It is by now widely accepted that strong correlation effects often present in this family of materials are at the origin of their fascinating electrical and magnetic properties. However, their inherent complexity does not favor the pursued overall understanding of the microscopic electronic processes that determine such a rich variety of behaviors.

Metal-to-insulator (MI) transitions, in particular, are a rich source of information on the fundamental electronic energies determining the conductivity and nature of the relevant bands in $3d$ transition-metal compounds. The Mott¹ and Hubbard² approaches have been successfully applied, especially to the early (Ti-Cr) TM compounds.³ On another hand, the late transition-metal oxides such as the nickelates and cuprates are believed not to be of the Mott-Hubbard class but of a charge-transfer CT type,⁴ characterized by an oxygen $2p$ -like band (higher in energy than the lower Hubbard band) and a $3d$ -like upper Hubbard conduction band.

Within this context, the simple perovskites $R\text{NiO}_3$ ($R = \text{La, Pr, Nd, Sm, } \dots$) are very appealing and have stimulated great interest, since they were proposed as paradigmatic examples of CT insulators. They are the only known transition-metal oxides located at the boundary that separates "low- Δ metals" from "charge-transfer insulators" in the framework developed by Zaanen, Sawatzky, and Allen.^{4,5}

They undergo a first-order MI transition at a characteristic temperature that depends on the degree of distortion of the perovskite structure.^{6,7} Very little work, however, was done on their properties before 1991,⁸ basically because of the difficulty of their preparation, since elevated temperatures and high oxygen pressures are required to stabilize the Ni^{III} ion.

In Ref. 6 we broached the structural evolution across the MI transition of the pure nickel perovskites $R\text{NiO}_3$, giving evidence of subtle structural anomalies accompanying the electronic localization. It was thus shown that the transition from a delocalized behavior of $3d$ electrons into an insulating state is followed by an abrupt but very slight variation in the lattice parameters. Such variation in the expression of changes in the structural arrangement that basically consist of an isotropic expansion of the Ni-O bond given by $\Delta d_{\text{Ni-O}} \approx +0.004$ Å ($\text{M} \rightarrow \text{I}$). This modification accounts for the observed volume expansion at T_{MI} : $\Delta V/V \approx 0.25\%$. Moreover, the concomitant displacement of oxygen atoms causes in its turn sudden and coupled tilts of the NiO_6 octahedra, which result in the bending of the Ni-O-Ni angle (θ , $\Delta \theta \approx -0.5^\circ$) and, apparently, the narrowing of the conduction band below its critical value.

In addition, the electronic localization in PrNiO_3 and NdNiO_3 is followed by an unusual overall antiferromagnetic ground state of wave vector $\mathbf{k} = (1/2, 0, 1/2)$, with alternated ferromagnetic (F) and antiferromagnetic (AF) couplings that suggest a nonuniform orbital distribution of the single e_g electron.⁹

The investigation of the undoped nickelates has been extended to specimens where the R^{3+} site is partially occupied by divalent and tetravalent ions. In the present work, the combination of structural and electrical measurements in electron- and hole-doped $R_{1-x}A_x\text{NiO}_3$ perovskites has al-

lowed us to examine the transition temperatures of a large list of nickelates, where Ni has the formal valence “ $(3+x)$ ” or “ $(3-x)$ ” ($x \leq 0.10$). But, in addition, they have permitted us to isolate different contributions controlling the metal-to-insulator transition temperature. The paper is organized as follows: Section II is devoted to experimental details about sample preparation and x-ray, neutron, and resistivity measurements. Structural data, which show a contraction/expansion of the cell volume and the Ni–O bond upon hole/electron doping, are given in Sec. III, where the consequences of doping on the transport properties are also illustrated. Finally, in Sec. IV, we combine the structural and transport data in order to isolate the pure electronic effects on T_{MI} from secondary contributions such as the R -size effects. Interestingly, a remarkable electron-hole asymmetry is found in the stabilization of the metallic state by doping.

II. EXPERIMENT

The synthesis of the $RNiO_3$ family is not straightforward, since elevated temperatures and high oxygen pressures are required in order to obtain well-crystallized samples with narrow diffraction peaks.^{7,10,11} All the powder samples of $R_{1-x}A_xNiO_3$ investigated ($R=La,Nd$; $A=Sr,Ca,Th$; $0 \leq x \leq 0.10$) were prepared by the liquid-mix technique.¹¹ Stoichiometric amounts of analytical grade R_2O_3 and the nitrates $Ni(NO_3)_2 \cdot 6H_2O$ and $Ca(NO_3)_2$, $Sr(NO_3)_2$, or $Th(NO_3)_4 \cdot 5H_2O$ were solved in citric acid. Then, the citrate solution was dried and slowly decomposed by heating up to 600 °C. The intimate mixture of oxides was fired in air at 800 °C for several hours. The black precursor powders were then pressed into pellets and heated at 1000 °C under 200 bars of oxygen pressure for 12 h. Finally, they were slowly cooled (600 °C/h) down to room temperature (RT). X-ray-diffraction patterns were collected at RT in a Siemens D-501 goniometer. The fine structural details of several samples were also investigated by means of neutron diffraction at RT on the diffractometer DN5, equipped with a position sensitive detector, at the Siloé reactor of the Centre d’Etudes Nucléaires, in Grenoble. The 800 positional detectors of DN5 covered a range of 80° in 2θ , and the wavelength used was $\lambda = 1.345$ Å. We applied the Rietveld method to the diffraction patterns by using the FULLPROF program.¹² This characterization confirmed that all the samples were well crystallized and single phase. The oxygen content was found to be the nominal, within the calculated standard errors (1% for oxygen occupancy), in the refinement of the neutron data, in accordance with the thermogravimetric analysis reported by Alonso, Martínez-Lope, and Hidalgo in Ref. 11. Resistivity measurements were carried out on sintered pellets by conventional four-probe method in a He closed-cycle cryostat in the 11–300 K temperature range. Cooling and heating rates were the same in all the electrical measurements (0.3 K/min). The measuring current was 1 mA, and the current polarity was inverted in order to correct the offset of the amplifiers and thermoelectric contributions.

III. RESULTS

We show in Fig. 1 the x-ray-diffraction patterns of $Nd_{0.95}A_{0.05}NiO_3$ samples ($A=Ca, Sr, \text{ and } Th$) obtained at RT.

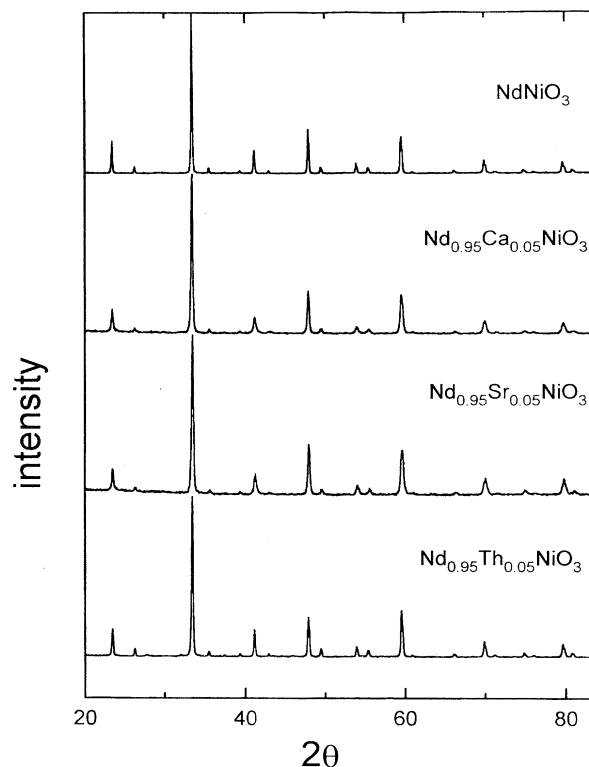


FIG. 1. X-ray-diffraction patterns of $NdNiO_3$, hole-doped $Nd_{0.95}Ca_{0.05}NiO_3$ and $Nd_{0.95}Sr_{0.05}NiO_3$, and electron-doped $Nd_{0.95}Th_{0.05}NiO_3$ at RT, all of them having the $Pbnm$ orthorhombic structure.

All the samples investigated have the orthorhombically distorted perovskite structure of the space group $Pbnm$. The only exception are the specimens containing the larger ion La, which are rhombohedrally distorted (space group $R\bar{3}c$). The refined lattice parameters are listed in Table I, together with the mean effective ionic radii of atoms at the rare-earth site. In the La compounds the refined parameters are referred to the hexagonal description of the $R\bar{3}c$ symmetry. Examination of the diffraction profiles confirmed that all the samples are well crystallized. The only difference between pure and doped samples is a very slight extra broadening of the reflections in the latter. This is probably due to the disorder-induced at the rare-earth sites in the doped perovskites, which are populated by R^{3+} and A^{2+}/A^{4+} ions. The oxygen pressure and temperature used (200 bars and 1000 °C) were enough to incorporate the bivalent and tetravalent ions into the structure, and we did not detect secondary phases in the diffraction patterns. The analysis of the neutron-diffraction data of $Nd_{0.95}Sr_{0.05}NiO_3$ and $Nd_{0.95}Th_{0.05}NiO_3$ obtained at RT on DN5 allowed us to survey fine structural details in these 5% electron and hole-doped samples, in particular, oxygen positions and distances. Refinement of the occupation factors of the oxygen sites led to the nominal oxygen stoichiometry within the standard error of ≈ 0.03 for the overall oxygen content. The refined atomic positions in the 5% doped samples, together with the isotropic temperature factors are listed in Table II. In the

TABLE I. Effective ionic radii at the rare-earth site (R_0), lattice parameters and cell volume of pure and doped $R_{1-x}A_x\text{NiO}_3$ (R : La,Nd; A : Ca^{2+} , Sr^{2+} , Th^{4+}).

	R_0 (Å)	Space group	a (Å)	b (Å)	c (Å)	V (Å ³)
LaNiO_3	1.160	$R\bar{3}c$	5.4573(1)	5.4573(1)	13.1462(3)	339.06(2)
$\text{La}_{0.90}\text{Sr}_{0.1}\text{NiO}_3$	1.170	$R\bar{3}c$	5.4455(3)	5.4455(3)	13.1600(9)	337.97(5)
$\text{La}_{0.90}\text{Th}_{0.10}\text{NiO}_3$	1.149	$R\bar{3}c$	5.4561(4)	5.4561(4)	13.155(1)	339.15(5)
NdNiO_3	1.109	$Pbnm$	5.3895(3)	5.3774(2)	7.6079(3)	220.48(6)
$\text{Nd}_{0.99}\text{Sr}_{0.01}\text{NiO}_3$	1.110	$Pbnm$	5.3925(3)	5.3749(4)	7.6069(2)	220.47(2)
$\text{Nd}_{0.98}\text{Sr}_{0.02}\text{NiO}_3$	1.112	$Pbnm$	5.3900(2)	5.3736(3)	7.6068(3)	220.32(3)
$\text{Nd}_{0.97}\text{Sr}_{0.03}\text{NiO}_3$	1.113	$Pbnm$	5.3967(4)	5.3663(1)	7.6066(4)	220.28(5)
$\text{Nd}_{0.95}\text{Sr}_{0.05}\text{NiO}_3$	1.116	$Pbnm$	5.3949(1)	5.3671(9)	7.6119(2)	220.40(1)
$\text{Nd}_{0.90}\text{Sr}_{0.10}\text{NiO}_3$	1.124	$Pbnm$	5.4014(1)	5.3638(1)	7.6167(2)	220.67(1)
$\text{Nd}_{0.99}\text{Ca}_{0.01}\text{NiO}_3$	1.109	$Pbnm$	5.3900(2)	5.3759(3)	7.6064(2)	220.40(2)
$\text{Nd}_{0.98}\text{Ca}_{0.02}\text{NiO}_3$	1.109	$Pbnm$	5.3903(4)	5.3727(2)	7.6035(1)	220.20(5)
$\text{Nd}_{0.97}\text{Ca}_{0.03}\text{NiO}_3$	1.109	$Pbnm$	5.3920(1)	5.3700(9)	7.6023(1)	220.12(9)
$\text{Nd}_{0.95}\text{Ca}_{0.05}\text{NiO}_3$	1.109	$Pbnm$	5.3934(3)	5.3698(3)	7.6047(1)	220.24(3)
$\text{Nd}_{0.90}\text{Ca}_{0.10}\text{NiO}_3$	1.110	$Pbnm$	5.3968(8)	5.3688(1)	7.6102(2)	220.50(8)
$\text{Nd}_{0.97}\text{Th}_{0.03}\text{NiO}_3$	1.107	$Pbnm$	5.3879(6)	5.3890(4)	7.6108(3)	220.62(7)
$\text{Nd}_{0.95}\text{Th}_{0.05}\text{NiO}_3$	1.106	$Pbnm$	5.3911(8)	5.3890(4)	7.617(1)	221.29(8)
$\text{Nd}_{0.92}\text{Th}_{0.08}\text{NiO}_3$	1.104	$Pbnm$	5.3927(7)	5.3926(3)	7.620(1)	221.59(8)
$\text{Nd}_{0.90}\text{Th}_{0.10}\text{NiO}_3$	1.103	$Pbnm$	5.3924(9)	5.3950(6)	7.620(2)	221.7(1)

orthorhombic GdFeO_3 -type structure of the $Pbnm$ space group, the rare-earth atom and oxygen O(1) are at site (4c) ($x, y, 1/4$), while Ni occupies the (4b) position ($1/2, 0, 0$), and the second oxygen O(2) is placed on the general (x, y, z) position. In Table III there are summarized the main distances and angles of NdNiO_3 , $\text{Nd}_{0.95}\text{Sr}_{0.05}\text{NiO}_3$ and $\text{Nd}_{0.95}\text{Th}_{0.05}\text{NiO}_3$ calculated from the refined atomic coordinates given in Table II. The structural data on the pure compounds given in Tables I, II, and III were taken from our previous high-resolution neutron-diffraction study reported in Ref. 6.

Sr^{2+} , Ca^{2+} , and Th^{4+} ions replace at random the rare-earth site but keeping the orthoferrite structure without modi-

TABLE II. Refined structural positions and isotropic temperature factors of pure and 5% doped (electrons and holes) NdNiO_3 from neutron diffraction data at RT. Rare earth and O(1) are at (4c) ($x, y, 1/4$), Ni is at (4b) ($1/2, 0, 0$) and O(2) is in general (8d) (xyz) position.

		$\text{Nd}_{0.95}\text{Sr}_{0.05}\text{NiO}_3$	NdNiO_3	$\text{Nd}_{0.95}\text{Th}_{0.05}\text{NiO}_3$
Nd	x	0.998(2)	0.9941(8)	0.992(1)
	y	0.0312(7)	0.0343(3)	0.038(6)
O(1)	B (Å ²)	0.40(7)	0.61(3)	0.21(8)
	x	0.069(2)	0.070(1)	0.0711(3)
O(2)	y	0.495(1)	0.4921(7)	0.493(1)
	B (Å ²)	1.0(3)	0.76(5)	0.8(2)
O(2)	x	0.721(1)	0.7150(6)	0.711(2)
	y	0.2811(9)	0.2842(6)	0.287(2)
O(2)	z	0.0363(7)	0.0378(4)	0.0339(9)
	B (Å ²)	0.3(2)	0.88(4)	0.3(2)

fyng the crystalline symmetry. The distortion in the skeleton of the NiO_6 octahedra is expected to increase (more tilted octahedra) with decreasing the effective ionic radius of the rare-earth atoms. In other words, smaller atoms at the rare-earth site cause the bending of the bond angle Ni-O-Ni governing the transfer integral between Ni e_g and O $2p$ orbitals.^{6,13}

It is found that the incorporation of bivalent ions

TABLE III. Main interatomic distances (Å) and Ni-O-Ni bond angles (°) in $\text{Nd}_{0.95}\text{A}_{0.05}\text{NiO}_3$ ($A = \text{Nd}^{3+}, \text{Sr}^{2+}, \text{Th}^{4+}$).

	N_0	$\text{Nd}_{0.95}\text{Sr}_{0.05}\text{NiO}_3$	NdNiO_3	$\text{Nd}_{0.95}\text{Th}_{0.05}\text{NiO}_3$
$d_{\text{Ni-O}(1)}$	2	1.939(2)	1.940(1)	1.946(2)
$d_{\text{Ni-O}(2)}$	2	1.942(5)	1.939(2)	1.936(5)
$d_{\text{O}(2)}$	2	1.930(5)	1.947(3)	1.954(5)
$\langle d_{\text{Ni-O}} \rangle$		1.937(4)	1.942(2)	1.945(4)
$d_{\text{Nd-O}(1)}$	1	2.904(9)	2.944(4)	2.970(8)
$d_{\text{O}(1)}$	1	2.517(9)	2.496(4)	2.492(8)
$d_{\text{O}(1)}$	1	3.07(1)	3.049(7)	3.06(1)
$d_{\text{O}(1)}$	1	2.34(1)	2.360(7)	2.36(1)
$d_{\text{Nd-O}(2)}$	2	2.586(7)	2.584(4)	2.607(7)
$d_{\text{O}(2)}$	2	2.418(7)	2.384(3)	2.396(7)
$d_{\text{O}(2)}$	2	2.684(7)	2.677(4)	2.640(6)
$\langle d_{\text{Nd-O}} \rangle$		2.621(8)	2.614(5)	2.617(8)
$\text{Ni-O}(1)\text{-Ni}$	2	157.9(5)	157.4(2)	156.3(5)
$\text{Ni-O}(2)\text{-Ni}$	4	158.6(11)	156.8(5)	157.0(10)
$\langle \text{Ni-O-Ni} \rangle$		158.4(9)	157.0(4)	156.8(8)

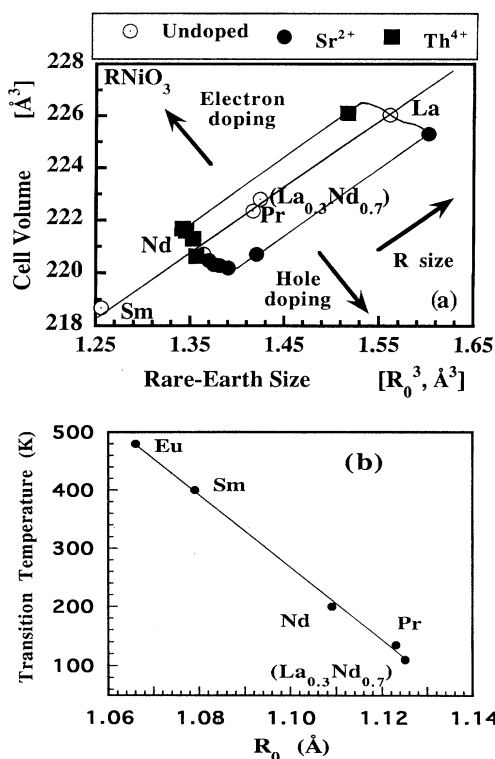


FIG. 2. (a) Expansion/contraction in the cell volume of $R_{1-x}A_x\text{NiO}_3$ (R : La,Nd; A : Th,Sr; $0 < x < 0.10$) due to electron/hole doping. The pure effect of the rare-earth size upon the volume is also shown. (The volume of La compounds is normalized to four formula units.) (b) Dependence of T_{MI} on the ionic radius of R in $R\text{NiO}_3$ compounds. The line is a linear fit to the data.

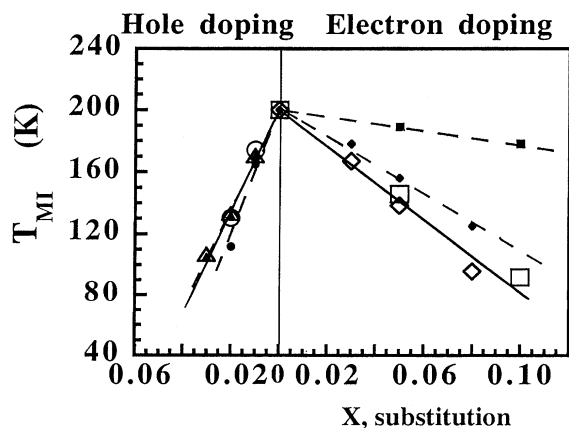


FIG. 3. Suppression of the metal-insulator transition (T_{MI}) in $\text{Nd}_{1-x}A_x\text{NiO}_3$ [A : Sr (circles), Ca (triangles), Ce (squares)] (from Ref. 14), and Th (rhombuses)] with electron and hole doping x . Closed symbols (dotted line) represent experimental values, whereas open symbols (full line) correspond to calculated T_{MI} , after subtracting R -size effects. Lines are guides to the eye.

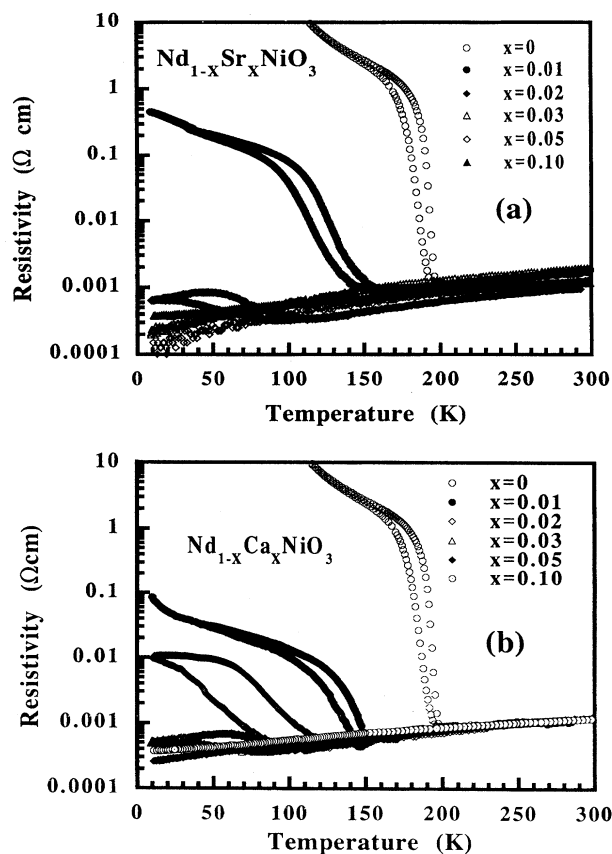


FIG. 4. Logarithmic resistivity vs temperature of $\text{Nd}_{1-x}A_x\text{NiO}_3$ perovskites with variable concentrations of divalent dopants: (a) $A = \text{Sr}^{2+}$, (b) $A = \text{Ca}^{2+}$ ($x = 0, 0.01, 0.02, 0.03, 0.05$, and 0.10). (The further right curves are the warming data.)

($\text{Sr}^{2+}, \text{Ca}^{2+}$) brings about a contraction of the unit cell, whereas doping with tetravalent ions (Th^{4+}) causes an expansion of the lattice [see Table I and Fig. 2(a)]. In Fig. 2(a) we have represented the volume of the unit cell in 16 pure

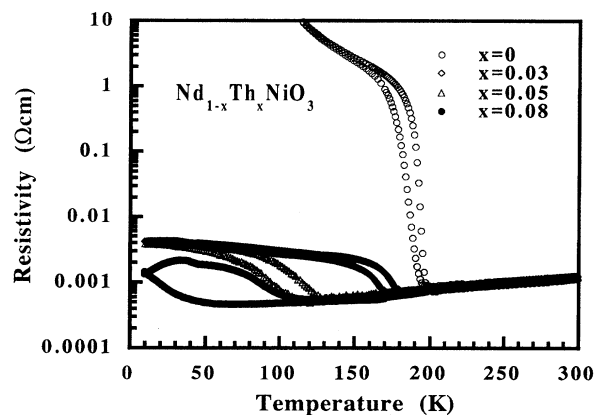


FIG. 5. Electrical resistivity ρ (in logarithmic scale) vs temperature of $\text{Nd}_{1-x}\text{Th}_x\text{NiO}_3$ for various concentrations of tetravalent doping ($x = 0, 0.03, 0.05$ and 0.08).

and doped nickelates versus their estimated effective rare-earth size. In this figure the volume of La compounds was normalized to the four formula units (f.u.) forming the orthorhombic cell (the rhombohedral cell of $\text{La}_{1-x}\text{A}_x\text{NiO}_3$ contains 6 f.u.). To be noted from a simple glance over Fig. 2(a) is that the modifications in the volume do not correspond to the steric changes expected regarding the effective rare-earth sizes (R_0). In fact, the changes in the samples with Sr or Th are opposite to those expected from consideration of their mean ionic radii. In the samples with bivalent dopants there is a contraction of the cell despite the larger effective size of Sr^{2+} , for instance, compared to La^{3+} or Nd^{3+} ($R_0[\text{Sr}^{2+}] = 1.26 \text{ \AA} > R_0[\text{La}^{3+}] = 1.16 \text{ \AA} > R_0[\text{Nd}^{3+}] = 1.11 \text{ \AA}$). On the other hand, the cell expands in the electron doped Th^{4+} -perovskites [Fig. 2(a)]. We recall that $R_0[\text{Th}^{4+}] = 1.05 \text{ \AA} < R_0[\text{Nd}^{3+}] = 1.11 \text{ \AA} < R_0[\text{La}^{3+}] = 1.16 \text{ \AA}$.

With respect to the transport measurements, partial replacement of Nd by bivalent or tetravalent ions results in a lowering of the transition temperature. The dependence of T_{MI} with doping is displayed in Fig. 3 for both cases. The abrupt change in the electrical resistivity at T_{MI} makes it easy to determine the transition temperature in the investigated compounds (see Figs. 4 and 5). Given that resistivity is hysteretic below T_{MI} , the transition temperatures have been determined upon heating measurements. While there is a progressive increase of the hysteresis range by doping, the temperature at which the slope of $\rho(T)$ changes from negative to positive in a heating procedure remains well defined in all the samples. We did not find measurable variations of T_{MI} with the heating rate of the sample. It is also found that the rate of phase transformation decreases with x in all the cases (electrons and holes), but neither depends simply on the unit-cell volume nor on the amount of extra charge injected in the Ni-O network. At the present stage, whether the width of the hysteresis loop is intrinsic to the material or is also controlled by granular effects is still unclear.

IV. DISCUSSION AND CONCLUSIONS

There is no doubt from these measurements that the Ni-O bands can actually be doped with either electrons and holes. The variations in the lattice parameters listed in Table I should be attributed to two separate effects that for some dopants act in opposite senses, namely, (i) size and (ii) intrinsic electronic effects. The cell volume of $R^{3+}_{0.9}\text{Sr}^{2+}_{0.1}\text{NiO}_3$ samples displays, when plotted versus the mean size $R_0^3[R_{1-x}\text{Sr}_x]$, a straight line parallel to the line determined by the linear increase with R_0^3 of the cell volume in the pure compounds. A similar evolution is found in the n -doped compounds $R^{3+}_{0.9}\text{Th}^{4+}_{0.1}\text{NiO}_3$ [see Fig. 2(a)]. What should be emphasized is that the straight lines of, nominally, equally hole-doped $R_{1-x}\text{A}_x\text{NiO}_3$ compounds (x fixed and R variable) fall below the line determined by the undoped Ni perovskites. This is so despite the larger size of Sr^{2+} compared to R^{3+} ($R_0[\text{Sr}^{2+}] = 1.26 \text{ \AA} > R_0[\text{La}^{3+}] = 1.16 \text{ \AA} > R_0[\text{Nd}^{3+}] = 1.109 \text{ \AA}$). Conversely, the corresponding lines defined by equally electron-doped nickelates fall above the line representing the pure oxides, and it should be recalled again that the ionic radius of Th^{4+} (1.05 \AA) in eight coordination is noticeably smaller than that of R^{3+} .

The observed cell expansion/contraction, then, cannot

be understood on the basis of steric effects associated with R_0 but is a consequence of the modification through doping of the Ni-O bonds. This essential point has been further confirmed by the detailed structural data gathered in Tables II and III for the 5% doped materials. The average Ni-O bondlength, respectively, decreases in $\text{Nd}_{0.95}\text{Sr}_{0.05}\text{NiO}_3$ [$d_{\text{Ni-O}} = 1.937(2) \text{ \AA}$] and increases in $\text{Nd}_{0.95}\text{Th}_{0.05}\text{NiO}_3$ [$d_{\text{Ni-O}} = 1.945(2) \text{ \AA}$] with respect to the pure compound NdNiO_3 [$d_{\text{Ni-O}} = 1.942(2) \text{ \AA}$]. These variations, of purely electronic origin, are accompanied by a straightening of the Ni-O-Ni angle (θ) in the Sr sample and an enhanced bending of θ in the Th^{4+} sample. At this point we call to mind that the Ni-O distance, as reported by us in Ref. 6, is not modified in the orthorhombic $R\text{NiO}_3$ cell when $R = \text{Nd}$ is substituted by Pr ($d_{\text{Ni-O}}[\text{Pr}] = d_{\text{Ni-O}}[\text{Nd}] = 1.942(2) \text{ \AA}$). Hence, the Ni-O bondlength is expected not to change with R_0 , and this fact reinforces the pure electronic origin of the systematic variations found in the NiO_6 octahedra by doping.

According to the Ref. 6, a good approximation to the relationship between small increments of the tolerance factor t and the Ni-O-Ni bond angle θ is given by

$$\Delta\theta \approx 275\Delta t \quad (\theta \text{ being the mean } \langle \text{Ni-O-Ni} \rangle \text{ angle}); \quad (1)$$

the tolerance factor in a perovskite ABO_3 being defined by

$$t = d_{A-O}/d_{B-O}\sqrt{2}. \quad (2)$$

Thus, differentiating Eq. (2) and substituting in (1), one obtains a relationship between small variations in the angle θ and the changes in d_{R-O} and $d_{\text{Ni-O}}$:

$$\Delta\theta \approx \frac{275}{\sqrt{2}} \left[\frac{\Delta d_{R-O}}{d_{\text{Ni-O}}} - \frac{d_{R-O}}{d_{\text{Ni-O}}^2} \Delta d_{\text{Ni-O}} \right]. \quad (3)$$

Now, we can apply Eq. (3) to the structural data in Table III for $\text{Nd}_{0.95}\text{Sr}_{0.05}\text{NiO}_3$ and $\text{Nd}_{0.95}\text{Th}_{0.05}\text{NiO}_3$. Experimentally, the difference of the bond angle between these samples is $(\Delta\theta)_{\text{expt}} = 158.4 - 156.8 = 1.6^\circ$. And, on another hand, the cation to oxygen instances differ by $\Delta d_{R-O} = 4 \times 10^{-3} \text{ \AA}$ and $\Delta d_{\text{Ni-O}} = -8 \times 10^{-3} \text{ \AA}$. Then, based on Eq. (3), our estimate of what should be the variation of the average Ni-O-Ni angle yields $\Delta\theta \approx 1.49^\circ$. This value is in excellent agreement with the measured change (1.6°). Consequently, in doped nickelates the changes observed in θ are well explained by a merely steric accommodation of the structure to the two relevant structural changes: namely, (a) the R -O distance, modified in virtue of the size of the atoms involved and (b) the electronically driven change in the Ni-O bondlength.

Next, we would like to focus our attention on the problem of the stabilization of the metallic state by doping. We will show that there is an electron-hole asymmetry in the suppression of the MI transition. The lowering of the MI transition temperature by doping is shown in Fig. 3 (closed symbols and dotted lines represent the experimental values). However, in addition to the extra carriers, size effects are also contributing to the final T_{MI} . Hereafter we must distinguish between the experimental $T_{\text{MI}}(x, R_0(x))$ (x is the substituted amount and R_0 is the mean rare-earth size) and $T'_{\text{MI}}(x)$, the first being the experimental value and the second the virtual transition temperature in NdNiO_3 after adding x carriers

TABLE IV. Suppression rates of T_{MI} for divalent ($A = \text{Sr}^{2+}, \text{Ca}^{2+}$) and tetravalent ($A = \text{Th}^{4+}, \text{Ce}^{4+}$) substitutions in $(\text{Nd}_{1-x}\text{A}_x)\text{NiO}_3$. dT_{MI}/dx is the experimental rate, and $\partial T_{\text{MI}}/\partial x$ is the rate calculated after R -size corrections (see explanation in the text).

	Hole doping		Electron doping	
	Sr	Ca	Th	Ce
$\left(\frac{dT_{\text{MI}}(x, R_0(x))}{dx}\right)_{x=0}$ $R_0 = R_0[\text{Nd}]$	-4190 K	-3180 K	-1029 K	-220 K
$\frac{dR_0(x)}{dx}$	0.151 Å	0.011 Å	-0.059 Å	-0.139 Å
$\left(\frac{\partial T_{\text{MI}}}{\partial x}\right)_{R_0 = R_0[\text{Nd}]}$ $x=0$	-3254 K	-3112 K	-1395 K	-1082 K
$\left(\frac{\partial T_{\text{MI}}}{\partial R}\right)_{x=0} \frac{dR_0(x)}{dx}$	-936 K	-68 K	366 K	862 K

(electrons or holes) per Ni ion to the Ni-O bands but keeping at the same time the average rare-earth size $R_0 = R_0[\text{Nd}]$. That is to say, size effects are not considered in $T'_{\text{MI}}(x)$ that only account for the carrier injection and the concomitant contraction/expansion of the Ni-O bond. In this approximation we can write

$$\left(\frac{dT_{\text{MI}}(x, R_0(x))}{dx}\right) = \left(\frac{\partial T_{\text{MI}}(x, R_0(x))}{\partial x}\right) + \left(\frac{\partial T_{\text{MI}}(x, R_0(x))}{\partial R_0}\right) \frac{dR_0(x)}{dx}. \quad (4)$$

This simple expression relates the observed changes in T_{MI} with the contributions from the extra carriers and size effects, separately. The left-hand side of Eq. (4) has been obtained experimentally for all the dopants by linear least-squares fitting of straight lines to the experimental values of T_{MI} as a function of x . A linear decrease of the transition temperature represents, for all the substitutional cations, a satisfactory approximation to the experimental data (see Fig. 3). Table IV lists the values of dT_{MI}/dx for the four dopants Sr, Ca, Th, and Ce (the data for Ce samples have been taken from Ref. 14). Moreover, the second term in the right-hand side of Eq. (4), representing R -size effects, can be also easily evaluated. The factor $\partial T_{\text{MI}}/\partial R_0$, by examining the experimental $T_{\text{MI}}(R_0)$ dependence, is shown to be linear in Fig. 2(b). Based on this figure we get $\partial T_{\text{MI}}/\partial R_0 \approx 6200 \text{ K}/\text{Å}$. The second factor, $dR_0(x)/dx$, was evaluated from the differences between the ionic radii of the dopants and Nd ions. In consequence, this procedure permitted us to finally estimate $\partial T_{\text{MI}}/\partial x$ on the right-hand side of Eq. (4), namely, the actual modification of the transition temperature exclusively due to carrier injection, without altering the rare-earth size. The values for $dR_0(x)/dx$ and $\partial T_{\text{MI}}/\partial x$ with $A = \text{Sr}, \text{Ca}, \text{Th},$ and Ce are listed in Table IV.

Enhanced R_0 values encompass the progressive straightening of the Ni-O-Ni angle and, thus, a positive variation of the free-carrier band-width with the corresponding lowering of the gap energy. However, based on the data gathered in Table IV, it becomes apparent that the primary cause for the stabilization of the metallic state by doping is not the modification of the rare-earth size (that plays an opposite role with $A = \text{Th}$ and Ce) but the incorporation of extra carriers. The decrease of the T_{MI} values is slightly more pronounced with Sr ($dT_{\text{MI}}/dx \approx -4190 \text{ K}$) than with Ca ($dT_{\text{MI}}/dx \approx -3180 \text{ K}$), and these differences are much more significant in the specimens doped with electrons: $dT_{\text{MI}}/dx \approx -1029 \text{ K}$ for Th and -220 K for Ce.

A central result of our study is the suppression of such differences after R -size corrections. Indeed, the bare suppression rates $\partial T_{\text{MI}}/\partial x$ obtained upon Sr and Ca substitution come to a very similar value: $(\partial T_{\text{MI}}/\partial x)_h \approx -3200 \text{ K}$. On the other hand, the right-hand side of Fig. 3 is even more meaningful, since size effects are rather more important with Ce^{4+} ions: the rate $dT_{\text{MI}}/dx \approx -220 \text{ K}$ is changed into $\partial T_{\text{MI}}/\partial x \approx -1082 \text{ K}$. Finally, a very similar bare rate is also found with Th. For electrons it is thus found that $(\partial T_{\text{MI}}/\partial x)_e \approx -1200 \text{ K}$.

In addition, the common suppression rates found in these hole- and electron-doped nickelates, separately, allows us to recalculate the metal-insulator transition temperatures in order to get T'_{MI} . The temperature at which electron localization would occur if extra carriers were injected in the Ni $3d$ -O $2p$ bands without modifying the sublattice of rare earth is, then,

$$T'_{\text{MI}} = T_{\text{MI}} + \left(\frac{\partial T_{\text{MI}}}{\partial x}\right)x. \quad (5)$$

The T'_{MI} values obtained using the above expression are represented with open symbols in Fig. 3, to be distinguished from T_{MI} (solid symbols). According to the above discussion,

the calculated values in the left (holes) and right (electrons) panels of Fig. 3 exhibit the linear dependence on x described by Eq. (5).

To be emphasized is that this interesting family of compounds constitute one of the very scarce opportunities to investigate the electron hole symmetry/asymmetry of charge-transfer TM oxides in the same crystalline structure. These Ni^{III} perovskites are able to incorporate both electrons and holes in TM-O bands. This is not possible in the cuprates $R_{2-x}A_x\text{CuO}_4$, for instance, where hole doping ($A = \text{Sr}^{2+}, \text{Ba}^{2+}, \dots$) is made in the so-called T structure, whereas doping with electrons requires the T' structure.¹⁵ Changes in the photoemission spectra of previously investigated charge-transfer oxides like the superconducting cuprates^{16,17} are not compatible with a rigid-band model in which E_F is systematically shifted. Carrier doping of RNiO_3 is expected to create new states within the charge-transfer band gap (midgap states) between the π^* ($\text{O } 2p - \text{Ni } t_{2g}$) valence band and σ^* ($\text{O } 2p - \text{Ni } e_g$) conduction band. We have found a significant electron-hole asymmetry in the bare suppression of T_{MI} by the extra carriers:

$$\left(\frac{\partial T_{\text{MI}}}{\partial x}\right)_{\text{holes}} \approx 3 \left(\frac{\partial T_{\text{MI}}}{\partial x}\right)_{\text{electrons}}.$$

The different nature of the respective midgap states is very likely at the origin of such asymmetry. Differences in the orbital symmetry of doped carriers should coexist with dif-

ferent couplings to the e_g^1 electron of the Ni^{III} ion. Doped holes probably have mainly $d^7\bar{L}$ character and are introduced on $\text{O } 2p^*$ orbitals with important contribution from Ni t_{2g} states. In the n -doped samples two electrons reside on e_g -like orbitals in the Ni²⁺ (d^8) state, and they are probably ferromagnetically coupled to form a high-spin state $S=1$. Whether doped holes form singlet states with the e_g^1 electrons deserves further investigation. It could well occur that the nonuniform orbital distribution of the single e_g electron⁹ might encompass that additional holes occupy different states, which could favor the itinerant motion.

In conclusion, these findings provide a simplified scenario of the influence of carrier injection upon the paradigmatic MI transition in RNiO_3 . The unequal dependence of T_{MI} on x for different dopants can be understood on the basis of an unified picture by separating R -size effects from carrier injection, and, in addition, we have found that holes are about three times more effective than electrons in closing the charge-transfer gap.

ACKNOWLEDGMENTS

We would like to acknowledge the CSIC-CIRIT and the Spanish DGICYT (Grant Nos. PB92-0849 and PB91-0089) for financial support, and M.S. would like to acknowledge a grant from the Spanish Ministerio de Asuntos Exteriores. The CENG is acknowledged for making available the neutron beam time.

¹N. F. Mott, Proc. Phys. Soc. London, Sec. A **62**, 416 (1949).

²J. Hubbard, Proc. R. Soc. London, Sec. A **277**, 237 (1964); **277**, 401 (1964).

³D. B. McWhan, J. P. Remeika, T. M. Rice, W. F. Brinkman, J. Maita, and A. Menth, Phys. Rev. Lett. **27**, 941 (1971).

⁴J. Zaanen, G. A. Sawatzky, and J. W. Allen, Phys. Rev. Lett. **55**, 418 (1985).

⁵J. B. Torrance, P. Lacorre, C. Ansavaroengchai, and R. M. Metzger, J. Solid State Chem. **90**, 168 (1991).

⁶J. L. García-Muñoz, J. Rodríguez-Carvajal, P. Lacorre, and J. B. Torrance, Phys. Rev. B **46**, 4414 (1992).

⁷P. Lacorre, J. B. Torrance, J. Pannetier, A. I. Nazzal, P. W. Wang, T. C. Huang, and R. L. Siemens, J. Solid State Chem. **91**, 225 (1991).

⁸G. Demazeau, A. Marbeuf, M. Pouchard, and P. Hagenmuller, J. Solid State Chem. **3**, 582 (1971).

⁹J. L. García-Muñoz, J. Rodríguez-Carvajal, and P. Lacorre, Phys. Rev. B **50**, 978 (1994).

¹⁰J. K. Vassiliou, M. Hornbostel, R. Ziebarth, and F. J. Disalvo, J. Solid State Chem. **81**, 208 (1989).

¹¹J. A. Alonso, M. J. Martínez-Lope, and M. A. Hidalgo, J. Solid State Chem. **116**, 146 (1995).

¹²J. Rodríguez-Carvajal (unpublished).

¹³J. B. Torrance, P. Lacorre, A. I. Nazzal, E. J. Ansaldo, and Ch. Niedermayer, Phys. Rev. B **45**, 8209 (1992).

¹⁴S. W. Cheong, H. Y. Hwang, B. Batlogg, A. S. Cooper, and P. C. Canfield, Physica B **194-196**, 1087 (1994).

¹⁵Y. Tokura, H. Takagi, and S. Uchida, Nature (London) **337**, 345 (1989).

¹⁶H. Romberg, M. Alexander, N. Nucker, P. Adelman, and J. Fink, Phys. Rev. B **42**, 8768 (1990).

¹⁷C. T. Chen *et al.*, Phys. Rev. Lett. **66**, 104 (1990); S. Uchida, T. Ido, H. Takagi, Y. Tokura, and S. Tajima, Physica B **165-166**, 1249 (1990).